Optical Response of High-Dielectric-Constant Perovskite-Related Oxide

C. C. Homes, *et al.*

Science **293**, 673 (2001);
DOI: 10.1126/science.1061655

Optical Response of High-Dielectric-Constant Perovskite-Related Oxide

C. C. Homes,[1]* T. Vogt,[1] S. M. Shapiro,[1] S. Wakimoto,[1,2]† A. P. Ramirez[3]

Optical conductivity measurements on the perovskite-related oxide $CaCu_3Ti_4O_{12}$ provide a hint of the physics underlying the observed giant dielectric effect in this material. A low-frequency vibration displays anomalous behavior, implying that there is a redistribution of charge within the unit cell at low temperature. At infrared frequencies (terahertz), the value for the dielectric constant is ~80 at room temperature, which is far smaller than the value of $\sim 10^5$ obtained at lower radio frequencies (kilohertz). This discrepancy implies the presence of a strong absorption at very low frequencies due to dipole relaxation. At room temperature, the characteristic relaxation times are fast (≲500 nanoseconds) but increase dramatically at low temperature, suggesting that the large change in dielectric constant may be due to a relaxor-like dynamical slowing down of dipolar fluctuations in nanosize domains.

Microelectronics is driven by an almost insatiable appetite for smaller and faster devices. In memory devices based on capacitive components, such as static and dynamic random access memories, the static dielectric constant ε_0 of a material will ultimately decide the degree of miniaturization. Perovskites possess high values for ε_0 and are widely used in such technological applications. The dielectric constant of a material is related to the polarizability α, in particular the dipole polarizability (an atomic property), which arises from structures with a permanent electric dipole that can change orientation in an applied electric field. These two quantities are linked through the Clausius-Mossotti relation. In metals, the charge is delocalized and $\varepsilon_0 \ll 0$. In insulators, the charge is localized and $\varepsilon_0 > 0$; materials with a dielectric constant greater than that of silicon nitride ($\varepsilon_0 > 7$) are classified as high-dielectric-constant materials. In general, a value of ε_0 above 1000 is related to either a ferroelectric that exhibits a dipole moment in the absence of an external electric field or to a relaxor characterized by a ferroelectric response under high electric fields at lower temperature, but no macroscopic spontaneous polarization. However, both classes of materials show a peak of ε_0 as a function of temperature, which is undesirable for many applications. For instance, capacitors [with capacitance $C = \varepsilon_0 A/d$; two plates of area A separated by a distance d] need to have static values to operate properly under a variety of conditions; if ε_0 has a strong temperature dependence, then the device will not be robust and may fail. Recently, the perovskite-related body-centered cubic (bcc) material $CaCu_3Ti_4O_{12}$ (CCTO) revealed an extraordinarily high dielectric constant at room temperature of $\sim 10^5$ (*1*, *2*) and was found to be practically constant between 100 and 600 K. Both properties are very important for device implementation (*3*, *4*). However, ε_0 displays a 1000-fold reduction below 100 K, without any detectable change of the long-range crystallographic structure when probed by high-resolution x-ray (*2*) and neutron powder diffraction (*1*). This is in marked contrast to known ferroelectrics (*5*, *6*), which structurally distort because of a soft-mode condensation. Here we present optical conductivity data and propose a mechanism for the physical origin of the large value of ε_0 and its 1000-fold drop of ε_0 below ~100 K.

Single crystals of CCTO were grown by the traveling-solvent floating-zone method in an image furnace. Dried starting materials of $CaCO_3$, CuO, and TiO_2 were mixed and heated at 800° and 850°C for 24 hours each, with intermediate grindings to make a single-phase powder of $CaCu_3Ti_4O_{12}$. For the initial growth, a ceramic rod was used as a seed. Each growth took ~8 hours, with the growth speed being 6 mm/hour in an oxygen atmosphere. During the growth, the upper and lower shafts were rotating at 30 rpm in opposite directions to each other in order to homogenize the molten zone. The typical size of the grown single crystals was ~5 mm in diameter and 20 mm in length. The $ACu_3Ti_4O_{12}$ family of compounds has been known for some time, and their structures have been determined (*7*) (Fig. 1).

A disc ~1 mm thick was cut from the middle of the boule with a wire saw. The front of the disc was then polished with successive laps to an optically flat mirrorlike surface. The temperature dependence of the real part of the complex dielectric function and the dissipation factor have been measured with a capacitive technique (*2*, *8*) at a number of different frequencies between 20 Hz and 1 MHz (Fig. 2, A and B, respectively). The static dielectric constant is taken as $\varepsilon_0 = \varepsilon_1(\omega \rightarrow 0)$, where the frequency-depen-

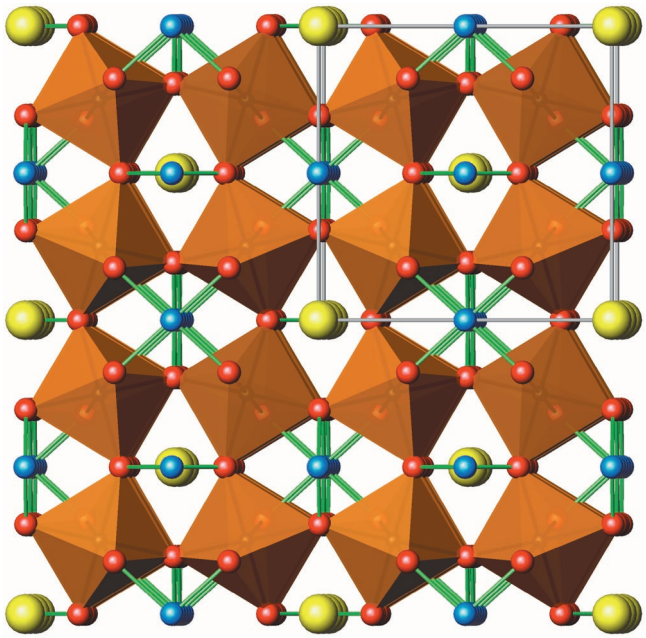

Fig. 1. Several unit cells of $CaCu_3Ti_4O_{12}$, shown as TiO_6 octahedra, Cu atoms (blue) bonded to four oxygen atoms (red), and large Ca atoms (yellow) without bonds.

[1]Department of Physics, Building 510B, Brookhaven National Laboratory, Upton, NY 11973–5000, USA. [2]Department of Physics, Massachusetts Institute of Technology, Cambridge, MA 02139–4307, USA. [3]Condensed Matter and Thermal Physics Group, MST-10 K764, Los Alamos National Laboratory, Los Alamos, NM 87545, USA.

*To whom correspondence should be addressed. E-mail: homes@bnl.gov

†Present address: Department of Physics, University of Toronto, 60 St. George Street, Toronto, Ontario, Canada, M5S 1A7.

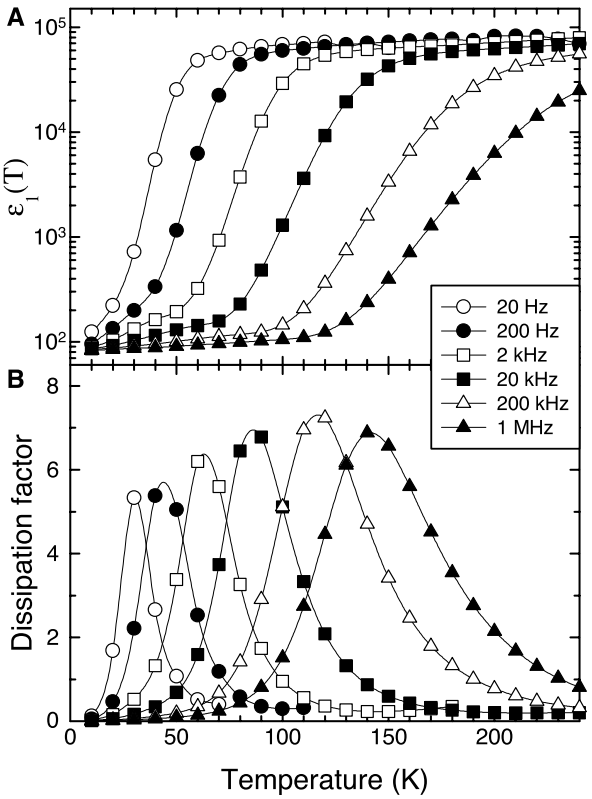

Fig. 2. (**A**) The temperature dependence of the real part of the dielectric response ε_1 of a single crystal of $CaCu_3Ti_4O_{12}$, at different frequencies between 20 Hz and 1 MHz. At 250 K, $\varepsilon_1 \sim 10^5$ below ~20 kHz; ε_1 decreases dramatically below ~100 K. (**B**) The temperature dependence of the dissipation factor (or loss component) of the dielectric response at the same frequencies.

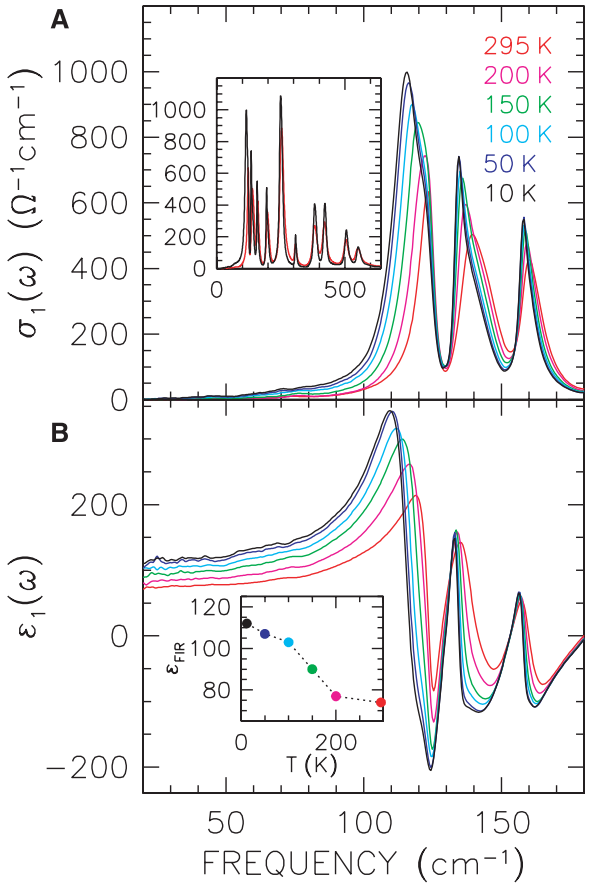

Fig. 3. (**A**) The temperature dependence of the real part of the optical conductivity $\sigma_1(\omega)$ of $CaCu_3Ti_4O_{12}$ from ~20 to 180 cm^{-1}. The low-frequency mode at ~122 cm^{-1} develops a shoulder at low temperature, indicative of splitting. The low-frequency mode also shows a dramatic increase in intensity at low temperature. This increase violates the *f*-sum rule and is an indication that there is a redistribution of charge within the unit cell. (Inset) The optical conductivity at 12 and 295 K shown over a wide frequency range. The optical conductivity is dominated by the infrared active lattice modes, which sharpen with decreasing temperature. Above ~300 cm^{-1}, the modes harden with decreasing temperature, whereas below this frequency, they soften instead. (**B**) The real part of the dielectric function $\varepsilon_1(\omega)$ of $CaCu_3Ti_4O_{12}$ in the far-infrared region for various temperatures. (Inset) The temperature dependence of the low-frequency value for the real part of the dielectric function $\varepsilon_{FIR} = \varepsilon_1(\omega \lesssim 20\ \text{cm}^{-1})$. At room temperature. $\varepsilon_{FIR} \sim 75$, which is far less than the value of ~10^5 observed in the Hz region and below. At low temperature, ε_{FIR} has increased to ~115, which is precisely the opposite to the decrease by ~1000 observed at low frequency. The opposite nature of these two trends suggests a strong absorption at low frequency at room temperature, which decreases rapidly with decreasing temperature.

dent complex dielectric function is $\tilde{\varepsilon}(\omega) = \varepsilon_1(\omega) + i\varepsilon_2(\omega)$, where $\varepsilon_1(\omega)$ and $\varepsilon_2(\omega)$ are the real and imaginary parts, respectively. The dissipation factor is also referred to as the loss tangent $\tan\delta = \varepsilon_2/\varepsilon_1$, where the angle δ is the phase difference between the applied electric field and the induced current (*9*). At 250 K, $\varepsilon_0 \sim 8 \times 10^4$ below 20 kHz; ε_0 decreases rapidly below ~100 K, a behavior that is also reflected in the shift of the peak in the dissipation factor. The real part of the dielectric function $\varepsilon_1(\omega)$ may also be determined from optical measurements; given the unusual temperature dependence of ε_0 at low frequency and the absence of any substantial structural distortion, the infrared study can provide important information as to the nature of this observation.

The temperature-dependent reflectance of CCTO was measured by means of an overfilling technique (*10*) over a wide frequency range (~20 to 16,000 cm^{-1}). The complex dielectric function has been determined from a Kramers-Kronig analysis of the reflectance. The temperature dependence of the real part of the complex conductivity $\tilde{\sigma}(\omega) = -i\tilde{\varepsilon}(\omega)/4\pi$ (Fig. 3A) in the low-frequency region, and over a wider region at room temperature and at 12 K in the inset, shows that the conductivity is dominated by relatively sharp peaks due to the infrared-active lattice vibrations. Above ~300 cm^{-1}, the lattice vibrations harden (shift to higher frequency) and narrow with decreasing temperature as expected due to anharmonicity, whereas the modes below this frequency soften (shift to lower frequency) dramatically. In addition, the mode at ~122 cm^{-1} develops a shoulder and displays an increase in oscillator strength below ~100 K (Fig. 3A). The complex dielectric function is modeled using Lorentzian oscillators

$$\tilde{\varepsilon}(\omega) = \varepsilon_\infty + \sum_j \frac{S_j\omega_j^2}{\omega_j^2 - \omega^2 - i\gamma_j\omega} \qquad (1)$$

where ω_j, γ_j, and S_j are the frequency, width, and dimensionless oscillator strength of the *j*th vibration, and ε_∞ is the core contribution to the dielectric function. Optical sum rules provide a powerful set of tools for examining the electronic properties of solids (*11*). If the overlap in $\sigma_1(\omega)$ between adjacent oscillators is negligible, as it appears to be in the present case (Fig. 3A), then the finite-energy conductivity sum rule for the *j*th Lorentzian oscillator is

$$\frac{120}{\pi}\int_{\omega_a}^{\omega_b} \sigma_1(\omega)d\omega = S_j\omega_j^2 \qquad (2)$$

where $\omega_a < \omega_j < \omega_b$; the interval $\omega_a \rightarrow \omega_b$ is chosen so that the full spectral weight of the *j*th oscillator is captured. This is better known as the *f*-sum rule. Thus, although the mode

may soften and narrow with decreasing temperature, the spectral weight (proportional to the integrated area under the peak, or $S_j\omega_j^2$), being a measure of the local coordination and bonding, should not change substantially. At room temperature, the oscillator strength for the mode at 122 cm^{-1} is $S = 14.4$. However, at 12 K this feature is best fit using a doublet consisting of a fundamental at 115 cm^{-1} and a shoulder at 121 cm^{-1}; fits to the conductivity result in an oscillator strength of the fundamental of $S = 46.8$, and $S' = 4.6$ for the shoulder. The overall increase in oscillator strength cannot be accounted for by the introduction of a new mode, and as a consequence, the *f*-sum rule is violated. This unequivocal signature may provide a first step to an understanding of this reduction of ε_0 observed in this material, because the violation of the *f*-sum rule has implications for the distribution of charge within the unit cell. In general, the evaluation of the effective charge of an ion is very difficult in systems with more than two types of atoms. For a material with k atoms in the unit cell, the effective charge per atom Z_k can be defined as (*12*)

$$\frac{1}{\varepsilon_\infty}\sum_j S_j\omega_j^2 = \frac{4\pi}{V_c}\sum_k \frac{(Z_k e)^2}{M_k} \qquad (3)$$

where $\Sigma_k Z_k = 0$ (as required by charge neutrality), V_c is the unit cell volume, and j and k index the lattice modes and the atoms with mass M_k, respectively. In many oxides, oxygen is often the lightest atom in the unit cell, and contributions from the heavier elements are often neglected in the summation, allowing the effective charge on the oxygen Z_0 to be approximated (*13*). The relatively light elements in CCTO complicate this approach. However, some general comments can still be made. The violation of the *f*-sum rule requires that the left side of Eq. 3 increase with decreasing temperature (from 4.78 × 10^6 cm^{-2} at 250 K to 5.23 × 10^6 cm^{-2} at 12 K, an increase of about 10%); to balance the relation, the values for Z_k must then also increase. Although it is difficult to say what the effective charge on a specific site will be, the overall effect is that the bonding becomes more ionic with decreasing temperature, and the increase in effective charge will be weighted toward the lighter elements, in particular the oxygen atoms. This is of particular importance for the TiO_6 octahedra, rather than the copper-oxygen sublattice. An increase in the effective charge on the oxygen atoms Z_0 and the subsequent change in the formal charge on the Ti atom should result in a different bond length. The covalent radii of Ti and O (1.36 and 0.73 Å, respectively) provide a simple estimate of 2.09 Å for the bond length, whereas the ionic radii of Ti and O (0.68 and 1.40 Å, respectively) give the nearly identical value of 2.08 Å (*14*). Thus, large changes in the formal charge are possible without associated commensurate structural changes. As the bonding in the TiO_6 octahedra becomes more ionic at low temperature, ε_0 is decreasing rapidly. Furthermore, the longer than expected Ca–O distance at low temperatures is also indicative of an increased ionicity (*1*).

The most interesting aspect of the optical properties is the temperature-dependent behavior of the real part of the dielectric function $\varepsilon_1(\omega)$ (Fig. 3B). In the far-infrared (FIR) region below the lowest measured lattice vibration, $\varepsilon_{FIR} = \varepsilon_1(\omega \lesssim 20\ cm^{-1})$ increases from ~70 at 295 K to ~120 at 10 K, as shown in the inset. The increase in ε_{FIR} with decreasing temperature is a consequence of the violation of the *f*-sum rule and the increase in the oscillator strengths of the infrared modes, as Eq. 1 shows in the limit of zero frequency

$$\varepsilon_0 = \varepsilon_\infty + \sum_j S_j \qquad (4)$$

The sum of the oscillator strengths of the infrared modes yields a value quite close to the observed value of ε_{FIR}, which is also in good agreement with the low-temperature value of ε_0. However, the trend in the far infrared down to ~20 cm^{-1} (2.5 meV or about 600 GHz) is for ε_{FIR} to increase with decreasing temperature; this is the opposite of the dramatic decrease observed in ε_0 below ~100 K (Fig. 2A). In order to reconcile the behavior of the optical properties with ε_0, Eq. 4 infers the existence of a strong absorption at very low frequencies. However, attempts to model the low-frequency behavior of ε_0 using the Lorentz model result in a severely overdamped oscillator ($\gamma \gg \omega_0$), implying that this process is dominated by relaxation effects ($\gamma = 1/\tau$) (*2*).

The suggestion that the physical processes in this system are dominated by relaxation effects naturally favors a Debye model (*9*) for the relaxation time of a dipole $P(t) = P_0 e^{-t/\tau}$, where P_0 is the dipole moment and τ is the characteristic relaxation time. The frequency response for the dielectric function is then

$$\tilde{\varepsilon}(\omega) = \varepsilon_\infty + \frac{P_0\tau(1 + i\omega\tau)}{1 + (\omega\tau)^2} \qquad (5)$$

and $P_0\tau = \varepsilon_0 - \varepsilon_\infty$. The temperature dependence of the dielectric constant at fixed frequencies in Fig. 2A has been replotted to illustrate the frequency dependence of this quantity at fixed temperatures in Fig. 4A. The Debye model has been used to model the frequency dependence of this quantity, and the fits are indicated by the solid lines. Although there is some uncertainty in the value of τ at high and low temperatures, in general the model fits are quite good. The surprising result from these fits is the large change in the relaxation rate τ. The rapid decrease of τ with

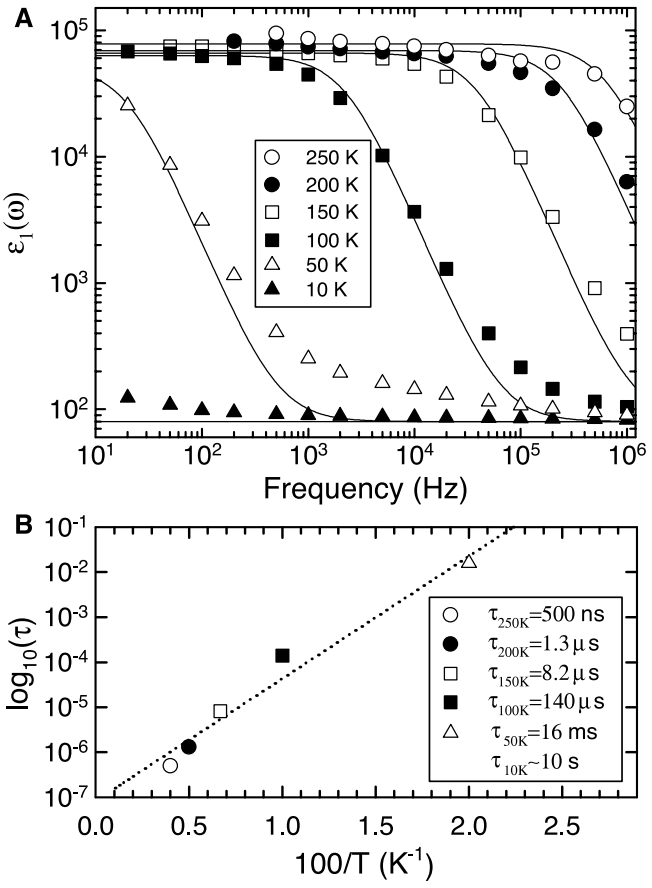

Fig. 4. (**A**) The frequency dependence of the dielectric constant ε_1 of $CaCu_3Ti_4O_{12}$ (measured at a large number of frequency points between 20 Hz and 1 MHz), shown for several temperatures. The solid lines represent the calculated values, assuming a Debye model using $\varepsilon_\infty = 80$; at 150 K, the model parameters are $\tau \sim 8.2$ μs and $P_0\tau = \varepsilon_0 - \varepsilon_\infty \sim 8 \times 10^4$. The relaxation times are quite short at high temperature and increase dramatically at low temperature. (**B**) The log of the relaxation time τ versus $1/T$, which shows activated behavior $\tau = \tau_0 \exp(U/k_BT)$; a linear regression of the data (dotted lines) yields the values $U = 54$ meV (630 K) and $\tau_0 \sim 84$ ns. The legend also gives the estimated relaxation time at 10 K, which is not shown on the plot.

increasing temperature is suggestive of an increasing dipole density and a faster polarization process

$$\tau = \tau_0 \exp(U/k_B T) \quad (6)$$

(k_B, Boltzmann constant). A linear regression of log τ versus $1/T$ (Fig. 4B) describes the data quite well, as indicated by the dotted line, and yields $U = 54$ meV (630 K) and $\tau_0 = 84$ ns. For 100 K $\lesssim T \lesssim U$, ε_0 is approximately constant, but for $T \gtrsim U$, the dielectric constant begins to increase rapidly to over 3×10^5 in the ceramic materials at ~400°C (~670 K) (*1*).

Subramanian *et al.* (*1*) speculate that the high dielectric constant of this material is enhanced by its microstructure because of the creation of an effective circuit of parallel capacitors, as found in boundary-layer dielectrics (*15*). The recurring observation of twinned single crystals at very small length scales suggests this as a possible mechanism to create barrier layer capacitances at the twin boundaries, thereby enhancing ε_0.

The origin of the large dipole moments P_0 is still uncertain at this time. Polar domains could be induced by local distortions, due to, for example, symmetrical off-center Ti displacements along the eight <111> directions, as is common in TiO_6-containing compounds. However, it is surprising that, unlike in other stoichiometric titanates, a ferroelectric transition is not observed. Rather, the electric dipoles freeze through a relaxational process; at low temperatures, one observes a relaxor-like slowing down of the dipole fluctuations as evidenced by the dramatic increase in τ and a dramatic decrease in ε_0. A clue to the large dielectric constant comes from its near temperature-independence at high temperatures, which implies that the correlation length does not grow on cooling as in conventional ferroelectrics. Further, it is unusual that the changes in bonding within the TiO_6 octahedron do not distort the structure, as is usually observed in perovskite compounds; the bcc structure persists down to low temperature. At present, these results suggest that the octahedral tilt (Fig. 1) is large enough to accommodate local distortions, thus effectively decoupling the ferroelectric order parameter and the crystal structure. Then, given the bcc structure, which prohibits ferroelectricity on symmetry grounds, the present results are consistent with a geometrical frustration of ferroelectric order (*1*).

References and Notes

1. M. A. Subramanian, Dong Li, N. Duan, B. A. Reisner, A. W. Sleight, *J. Solid State Chem.* **151**, 323 (2000).
2. P. Ramirez *et al.*, *Solid State Commun.* **115**, 217 (2000).
3. R. Singh, R. K. Ulrich, *Electrochem. Soc. Interface* **8**, 26 (1999).
4. B.-G. Kim, S. M. Cho, T.-Y. Kim, H. M. Jang, *Phys. Rev. Lett.* **86**, 3404 (2001).
5. Z. Zeng, M. Greenblatt, M. A. Subramanian, M. Croft, *Phys. Rev. Lett.* **82**, 3164 (1999).
6. D. Bruce, R. A. Cowley, *Structural Phase Transitions* (Taylor & Francis, London, 1981).
7. X. X. Bochu, M. N. Deschizeaux, J. C. Joubert, *J. Solid State Chem.* **29**, 291 (1979).
8. The transport measurements were performed at Lucent Technologies, Bell Labs, 600 Mountain Avenue, Murray Hill, NJ 07974, USA.
9. V. V. Daniel, *Dielectric Relaxation* (Academic Press, New York, 1967), pp. 4–19.
10. C. C. Homes, M. Reedyk, D. A. Crandles, T. Timusk, *Appl. Opt.* **32**, 2972 (1993).
11. D. Y. Smith, in *Handbook of Optical Constants of Solids*, E. D. Palik, Ed. (Academic Press, New York, 1985), pp. 35–68.
12. J. F. Scott, *Phys. Rev. B* **4**, 1360 (1971).
13. S. Tajima *et al.*, *Phys. Rev. B* **43** 10496 (1991).
14. W. W. Porterfield, *Inorganic Chemistry, a Unified Approach* (Academic Press, New York, ed. 2, 1993); A. M. James, M. P. Lord, *Mcmillan's Chemical and Physical Data* (Macmillan, London, 1992); J. E. Huheey, E. A. Keiter, R. L. Keiter, *Inorganic Chemistry: Principles of Structure and Reactivity* (HarperCollins, New York, ed. 4, 1993).
15. C. F. Yang, *Jpn. J. Appl. Phys.* **36**, 188 (1996).

16. We thank D. Buttrey, J. F. Scott, A. W. Sleight, D. Vanderbilt, R. Werner, and P. Woodward for fruitful discussions. The work at Brookhaven was supported by the U.S. Department of Energy under contract no. DE-AC02-98CH10886. The work at MIT was supported by NSF under grant no. DMR0071256 and by the MRSEC Program of NSF under award no. DMR98-08941.

16 April 2001; accepted 26 June 2001

β-Helical Polymers from Isocyanopeptides

Jeroen J. L. M. Cornelissen,[1] Jack J. J. M. Donners,[3] René de Gelder,[2] W. Sander Graswinckel,[1] Gerald A. Metselaar,[1] Alan E. Rowan,[1] Nico A. J. M. Sommerdijk,[3] Roeland J. M. Nolte[1,3]*

Polymerization of isocyanopeptides results in the formation of high molecular mass polymers that fold in a proteinlike fashion to give helical strands in which the peptide chains are arranged in β-sheets. The β-helical polymers retain their structure in water and unfold in a cooperative process at elevated temperatures. The peptide architecture in these polymers is a different form of the β-helix motif found in proteins. Unlike their natural counterparts, which contain arrays of large β-sheets stacked in a helical fashion, the isocyanopeptide polymers have a central helical core that acts as a director for the β-sheet–like arrangement of the peptide side arms. The helical structure of these isocyanopeptide polymers has the potential to be controlled through tailoring of the side branches and the hydrogen-bonding network present in the β-sheets.

The two principal structural elements found in proteins are the α-helix and the β-sheet. In 1993, a new structural motif was discovered, the so-called β-helix, which was first observed in the bacterial enzyme *pectate lyase* (*1*). The β-helical architecture is constructed from polypeptides that are coiled into a large helix, formed by stacks of β-sheets separated by loops. β-Sheet helices are present in the fibrous form of *thransyretin*, which plays an important role in bovine spongiform encephalopathy (BSE) and Creutzfeld-Jacob diseases, type II diabetes, and Alzheimer's disease (*2*), and form the crucial structural elements in insect antifreeze proteins (*3*). We report on synthetic analogs of β-helices (*4*, *5*) that are formed by polymerization of isocyanopeptides (*6*).

Polymers of isocyanides are prepared by a nickel(II)-catalyzed reaction (*6*). They adopt a ~4_1 helical conformation (four repeats per turn) when bulky side groups are present [e.g., poly(*tertiary*-butylisocyanide)] (*7*). In the case of less sterically demanding side chains (*8*, *9*) (e.g., polyphenylisocyanide), the helical backbone slowly uncoils upon standing in solution (*10*). The helix sense of the backbone can be controlled with either optically active monomers or a chiral nickel catalyst (*6*). We describe the polymerization of isocyanopeptides leading to products in which the helical backbone is stabilized by hydrogen bonds between amide groups in parallel side chains (*11*). Each side chain can be regarded as an individual β-strand, and the overall arrangement of the side chains leads to a helical β-sheet–like organization. We prepared a series of polymers derived from L- and D-alanine–containing peptides (Fig. 1A) [see supplementary information (*12*)] to investigate the structural properties of these macromolecules, in particular the hydrogen-bonding patterns.

A β-sheet–like hydrogen-bonding array between stacked peptide strands is present in single crystals of the monomer L-isocyanoalanyl-L-alanine methyl ester (L,L-IAA; Fig. 1B). This results in a characteristic N-H stretching vibra-

[1]Department of Organic Chemistry, [2]Department of Inorganic Chemistry, University of Nijmegen, Toernooiveld 1, 6525 ED Nijmegen, Netherlands. [3]Laboratory for Macromolecular and Organic Chemistry, Eindhoven University of Technology, Post Office Box 513, 5600 MB Eindhoven, Netherlands.

*To whom correspondence should be addressed. E-mail: nolte@sci.kun.nl